Available online at www.sciencedirect.com
ScienceDirect
Journal of Sound and Vibration 308 (2007) 867–878
JOURNAL OF SOUND AND VIBRATION
www.elsevier.com/locate/jsvi

Modelling and analysis of omni-directional piezoelectric actuator

P. Vasiljev[a], D. Mazeika[b,*], G. Kulvietis[b]

[a]*Vilnius Pedagogical University, Studentu 39, LT-08106 Vilnius, Lithuania*
[b]*Vilnius Gediminas Technical University, Sauletekio av. 11, LT-10223 Vilnius, Lithuania*

Accepted 29 March 2007
The peer review of this article was organised by the Guest Editor
Available online 7 June 2007

Abstract

A study of a novel multi-degree-of-freedom piezoelectric actuator is given in the paper. Design of the actuator is based on the implementation of bending vibrations of a circular plate. The actuator consists of a vibrating disc with the driving tip mounted at the disc centre and a piezoceramic disc. This actuator can move a slider in two perpendicular directions in the plane and achieve a curvilinear or rotational motion of the positioned object depending on the excitation scheme of the electrodes. Numerical modelling based on the finite element method was performed to find resonant frequencies and modal shapes of the actuator and to calculate the trajectories of contact point's movements under different excitation schemes. The transient dynamic analysis of the actuator was performed to simulate the motion of the slider. A contact between the driving tip, slider and slider-way was taken into account in the finite element model. A prototype actuator was made and measurement results of actuator's top surface's oscillations are given. Results of the numerical and experimental investigation are analysed and discussed.

1. Introduction

Piezoelectric actuators are widely used in the development of nano/micro positioning and manipulation systems. These actuators are capable to reach the high resolution and speed of the positioning object and possess many attractive features such as a short response time, a large output power, a compact size, self-braking and good controllability [1–3]. Most of piezoelectric actuators are single degree-of-freedom (DOF) devices: it means that actuators generate a one-dimensional linear or rotational motion of the moving part [3,4]. Only few multi-degree-of-freedom actuators are developed that are capable to actuate in many directions [4–7]. Usually, mechanical systems composing several actuators are used for two-dimensional (2D) or three-dimensional (3D) positioning of the object, that is, each DOF uses separate actuator [4,8]. Accuracy of the positioning reduces applying this design principle to mechanical systems. Obviously, the best way is to use omni-directional piezoelectric actuator that can move or rotate the body in any direction.

*Corresponding author. Tel.: +370 5 2744913: fax: +370 5 2700112.
E-mail address: Dalius.Mazeika@fm.vtu.lt (D. Mazeika).

0022-460X/$ - see front matter © 2007 Elsevier Ltd. All rights reserved.
doi:10.1016/j.jsv.2007.03.074

A novel design of a multi-degree-of-freedom piezoelectric actuator based on shaking beam principle [9] is proposed and analysed in this paper. The actuator realises a possibility to move objects in a 2D or 3D space. Finite element modelling of the actuator is performed, and an experimental prototype is made. This newly developed piezoelectric actuator can be successfully used in sophisticated positioning or manipulating systems.

2. Operating principle of piezoelectric actuator

The design principle of the introduced piezoelectric actuator is based on a previous research of the shaking-beam type actuators [7,9] when bending modes of the disc are used. A configuration of the actuator includes following parts: a vibrating disc with the driving tip mounted at the disc centre and a piezoceramic disc. Both discs are glued together. Electrodes are located at the bottom area of the piezoceramic disc and are divided into four equal sectors. Polarization of piezoceramic is oriented along the thickness of the disc and d33 effect is used for the actuation.

An elliptic trajectory of the contact point motion is achieved when a combination of two bending modes of the vibrating disc is used. One bending mode must swing driving tip and another produce displacements perpendicular to the surface of the disc [5,6]. For the plate that is simply supported at the edges bending modes B21, B23, B43 can be used. These oscillation modes are achieved when a pair of two opposite electrodes is excited using sinusoidal voltage with the same frequency but different phases shifted by $\pi/2$. A schematic actuator and configuration of electrodes are shown in Fig. 1.

The configuration of electrodes allows using different excitation schemes of the actuator by varying an input voltage amplitude and phase and to obtain oscillation modes of the vibrating disc with nodal diameters rotated by different angles. The direction of a nodal diameter coincides with the direction of the main axis of

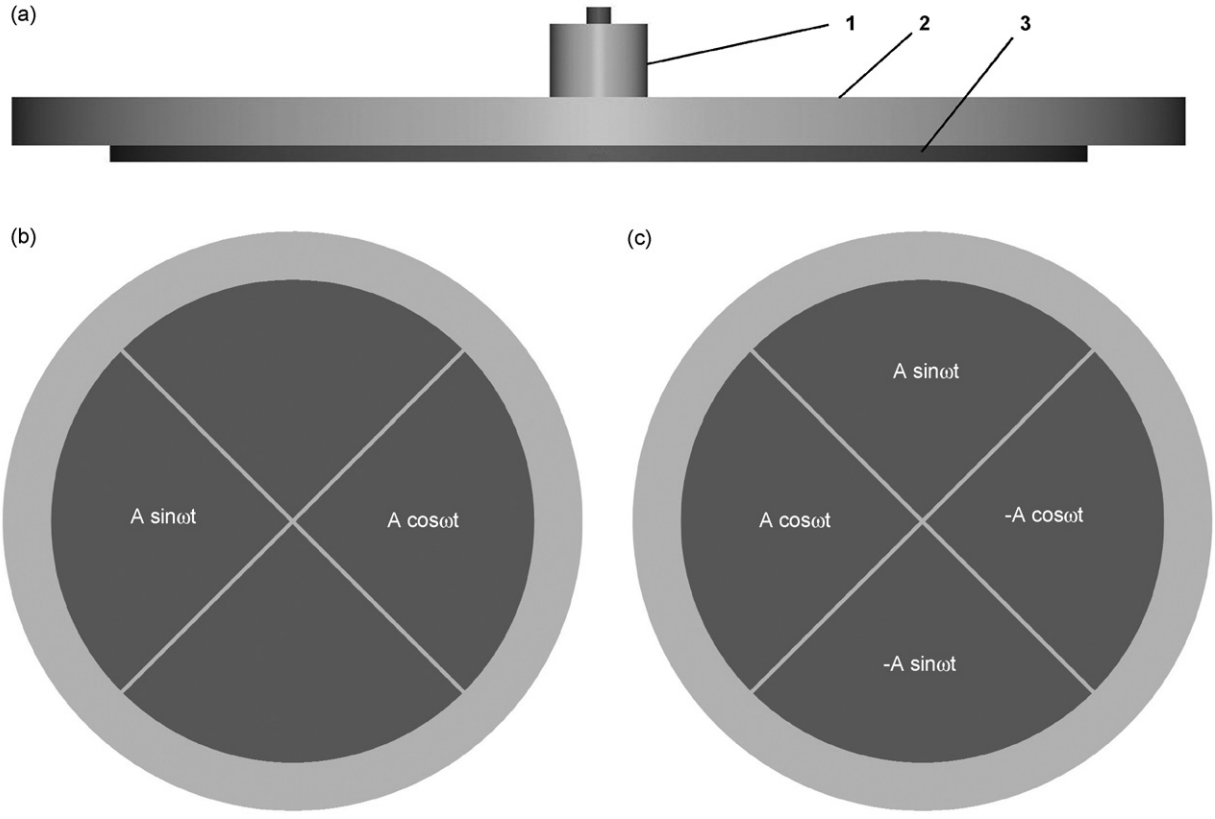

Fig. 1. (a) Schematic piezoelectric actuator: 1—driving tip and contact point, 2—vibrating disc, 3—piezoceramic disc; excitation scheme for slider movement parallel to x-axis (b) and for rotation about z-axis (c).

the contact point's elliptical motion and shows the direction of the slider movement. So it is possible to achieve an omni-directional movement of the slider in the plane using this piezoelectric actuator. Two excitation schemes are analyzed in the paper as shown in Figs. 1b and c. These schemes are used for linear and rotational motions of the slider.

3. FEM equations for actuator modelling

The finite-element method (FEM) was used to perform modal frequency, harmonic response and transient dynamic analysis, to calculate trajectories of the driven tip and slider and to find admittance dependence on the input voltage frequency. Basic dynamic equations of the piezoelectric actuator are derived from the principle of minimum potential energy by means of variational functionals and can be written as follows [7,8]:

$$\begin{cases} \mathbf{M}\ddot{\mathbf{u}} + \mathbf{C}\dot{\mathbf{u}} + \mathbf{K}\mathbf{u} + \mathbf{T}\boldsymbol{\varphi} = \mathbf{F}, \\ \mathbf{T}^{\mathrm{T}}\mathbf{u} - \mathbf{S}\boldsymbol{\varphi} = \mathbf{Q}, \end{cases} \tag{1}$$

where $\mathbf{M}$, $\mathbf{K}$, $\mathbf{T}$, $\mathbf{S}$, $\mathbf{C}$ are matrices of mass, stiffness, electroelasticity, capacity and damping, respectively; $\mathbf{u}$, $\boldsymbol{\varphi}$, $\mathbf{F}$, $\mathbf{Q}$ are, respectively, vectors of nodes displacements, potentials, external mechanical forces and charges coupled on the electrodes.

The driving force of the actuator is obtained from the piezoceramic disc. Finite-element discretisation of the disc consists of elements with the nodes coupled with electrodes that have the known values of electric potential. The nodal electric potential of remaining elements is calculated during solution. The dynamic equation of the piezoelectric actuator in this case can be expressed as follows [7,8]:

$$\begin{cases} \mathbf{M}\ddot{\mathbf{u}} + \mathbf{C}\dot{\mathbf{u}} + \mathbf{K}\mathbf{u} + \mathbf{T}_1\boldsymbol{\varphi}_1 + \mathbf{T}_2\boldsymbol{\varphi}_2 = \mathbf{F}, \\ \mathbf{T}_1^{\mathrm{T}}\mathbf{u} - \mathbf{S}_{11}\boldsymbol{\varphi}_1 - \mathbf{S}_{12}\boldsymbol{\varphi}_2 = \mathbf{Q}_1, \\ \mathbf{T}_2^{\mathrm{T}}\mathbf{u} - \mathbf{S}_{12}^{\mathrm{T}}\boldsymbol{\varphi}_1 - \mathbf{S}_{22}\boldsymbol{\varphi}_2 = \mathbf{0}, \end{cases} \tag{2}$$

here

$$\mathbf{T} = \begin{bmatrix} \mathbf{T}_1 & \mathbf{T}_2 \end{bmatrix}, \quad \mathbf{S} = \begin{bmatrix} \mathbf{S}_{11} & \mathbf{S}_{12} \\ \mathbf{S}_{12}^{\mathrm{T}} & \mathbf{S}_{22} \end{bmatrix}, \tag{3}$$

where $\boldsymbol{\varphi}_1$, $\boldsymbol{\varphi}_2$ are, respectively, the vector of nodal potentials of nodes coupled with electrodes and the vector of nodal potentials calculated during numerical simulation.

Mechanical and electrical boundary conditions are determined for the piezoelectric actuator, i.e. mechanical displacements and velocities of the fixed surfaces of the actuator are equal to zero and the electric potentials of the nodes that are not coupled with electrodes are equal to zero as well.

Natural frequencies and modal shapes of the actuator are derived from the modal solution of the piezoelectric system:

$$\det\left(\mathbf{K}^* - \omega^2\mathbf{M}\right) = \mathbf{0}, \tag{4}$$

where $\mathbf{K}^*$ is a modified stiffness matrix. In the case when $\mathbf{Q}_1 = 0$ it can be written as follows:

$$\mathbf{K}^* = \mathbf{K} + \mathbf{T}\mathbf{S}^{-1}\mathbf{T}^{\mathrm{T}}. \tag{5}$$

In the case when $\boldsymbol{\varphi}_1 = 0$ the modified stiffness matrix is

$$\mathbf{K}^* = \mathbf{K} + \mathbf{T}_2\mathbf{S}_{22}^{-1}\mathbf{T}_2^{\mathrm{T}}. \tag{6}$$

Harmonic response analysis of the piezoelectric actuator is carried out applying sinusoidal varying voltage with different phases on electrodes. Due to the inverse piezoelectric effect corresponding mechanical forces are obtained:

$$\mathbf{F}_1 = -\mathbf{T}\boldsymbol{\varphi}_1, \tag{7}$$

here a vector of nodal potentials $\boldsymbol{\varphi}_1$ can be written as

$$\boldsymbol{\varphi}_1 = \mathbf{U}\sin(\omega_k t), \tag{8}$$

where $\mathbf{U}$ is a vector of voltage amplitudes, applied to the nodes coupled with electrodes. Referring to Eqs. (2), (7) and (8), the vector of mechanical forces can be calculated as follows:

$$\mathbf{F}_1 = \left(\mathbf{T}_2\mathbf{S}_{22}^{-1}\mathbf{S}_{12}^{\mathrm{T}} - \mathbf{T}_1\right)\mathbf{U}\sin(\omega_k t). \tag{9}$$

Referring to Eq. (2) the vector of nodal charges $\mathbf{Q}_1$ can be written as follows:

$$\mathbf{Q}_1 = \left(\mathbf{T}_1^{\mathrm{T}} - \mathbf{S}_{12}\mathbf{S}_{22}^{-1}\mathbf{T}_2^{\mathrm{T}}\right)\mathbf{u} + \left(\mathbf{S}_{12}\mathbf{S}_{22}^{-1}\mathbf{S}_{12}^{\mathrm{T}} - \mathbf{S}_{12}^{\mathrm{T}}\right)\boldsymbol{\varphi}_1. \tag{10}$$

Results for structural displacements of the piezoelectric actuator obtained from harmonic response analysis are used to determine the trajectory of the contact point's movement. Admittance values on nodes of piezoceramic finite elements can be determined as the function of frequency:

$$Y_i = \frac{Q_i}{U_i}\omega e^{\mathrm{j}(\psi_i+\pi/2)}, \tag{11}$$

where j refers to the imaginary number, ψ is the phase. In order to find slider displacements, the contact between the driving tip, slider and slider-way must be taken into account and dynamic equations of motion of piezoelectric motor must be solved. FEM governing equations of the linear piezoelectric motor can be written as follows:

$$\begin{cases} \mathbf{M}\ddot{\mathbf{u}} + \mathbf{C}\dot{\mathbf{u}} + \mathbf{K}\mathbf{u} = \mathbf{F}_p + \mathbf{F}_c, \\ \mathbf{D}\dot{\boldsymbol{\delta}} + \mathbf{H}\boldsymbol{\delta} = \mathbf{F}_c, \\ \mathbf{m}\ddot{\boldsymbol{\delta}} + \mathbf{c}\dot{\boldsymbol{\delta}} = \mathbf{F}_f + \mathbf{F}_c, \end{cases} \tag{12}$$

where $\mathbf{F}_p$ is the vector of external mechanical forces generated by piezoelements; $\mathbf{F}_c$ is the vector of nodal contact forces; $\mathbf{F}_f$ is the vector of resistance forces of the slider, $\boldsymbol{\delta}$ is the vector of nodal displacements of the slider; $\mathbf{D}$, $\mathbf{H}$ are the damping and stiffness matrices of the contact surface.

4. Numerical modelling and simulation

Numerical modelling of the piezoelectric actuator was used to verify and validate its design and working principle through the modal, harmonic response and transient dynamic analysis. FEM package ANSYS 8.0 was employed in modelling and simulations.

4.1. Simulation of piezoelectric actuator

The finite-element model of the piezoelectric actuator consists of vibrating disc with the driven tip and piezoceramic disc as illustrated in Fig. 2. The model was built using 20-node structural solid brick elements SOLID95 and 10-node tetrahedral coupled-field solid elements SOLID98. SOLID95 elements were used to mesh the vibrating disc; the piezoceramic disc was meshed with SOLID98 elements. Material's properties used for actuator are listed in Table 1. Bronze was used for the vibrating disc, PZT-8 for the piezoceramic disc. An edge ring area at the bottom of the vibrating disc was mechanically constrained in x-, y- and z-directions.

Modal analysis of the piezoelectric actuator was done applying Block Lanczos eigenvalue solver. Damping was neglected in the finite element model. Resonant and anti-resonant frequencies of the actuator were calculated linked to electrical impedance. Analysing results it was determined that modes No. 2 (30.70 kHz) and No. 8 (60.99 kHz) can be used to move the slider. The first determined modal shape is B20 and the second B43. Modal shapes are shown in Fig. 3. Both modal shapes have nodal diameters and therefore driven tip is leaning towards the direction of slider movement.

Harmonic response analysis was performed with the aims to find out the actuator's response to sinusoidal voltage applied on electrodes of the piezoceramic disc and to calculate trajectories of the contact point's movement. Two excitation schemes were used in simulations as shown in Figs. 1a and b. A 30 V, AC signal was applied to electrodes. The movement of the slider towards the x-coordinate axis and rotation about

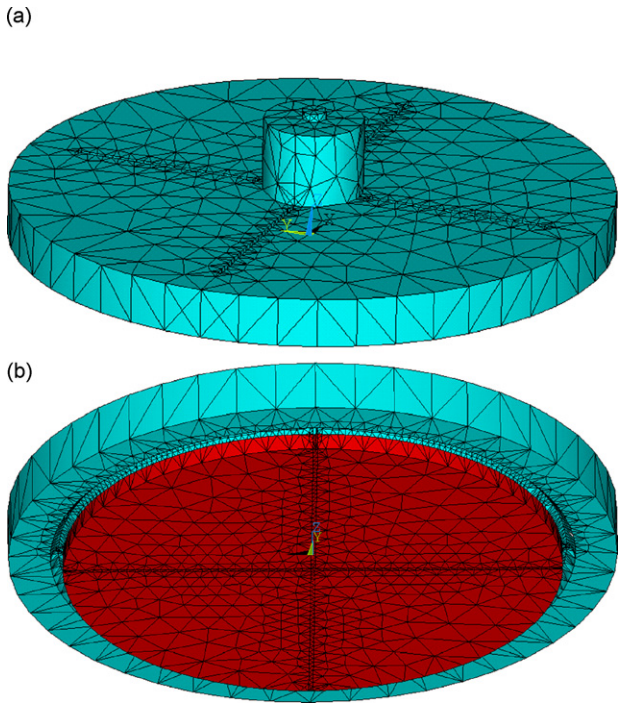

Fig. 2. Finite element model of actuator: (a) top view; (b) bottom view.

Table 1
Properties of the actuator materials

Material properties	Piezoceramic PZT-8	Bronze
Young's modulus (N/m^2)	8.5×10^{10}	1.15×10^{11}
Poison's ratio		0.307
Density (kg/m^3)	7600	8760
Permitivity, $\times 10^{-7}$(F/m)	$\varepsilon_{11} = 11.42$; $\varepsilon_{33} = 8.85$	
Piezoelectric matrix (C/m^2)	$e_{13} = -18.01$; $e_{33} = 29.48$; $e_{52} = 10.34$	
Elasticity matrix, $\times 10^{10}$ (N/m^2)	$c_{11} = 14.68$; $c_{12} = 8.108$; $c_{13} = 8.105$; $c_{33} = 13.17$; $c_{44} = 3.29$; $c_{66} = 3.14$	

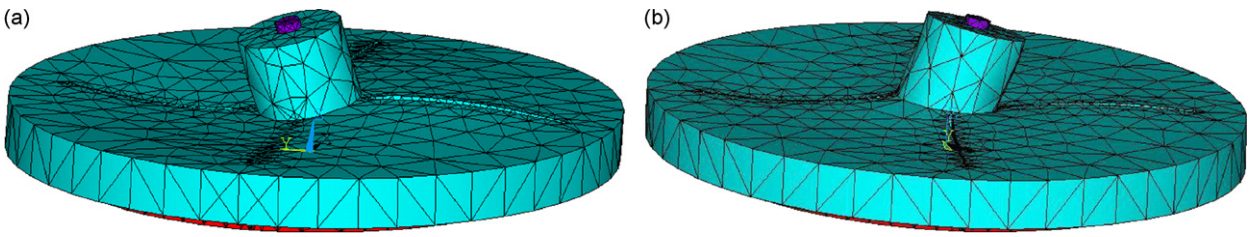

Fig. 3. Modal shapes of actuator: (a) No. 2 (30.70 kHz); (b) No. 8 (60.99 kHz).

the z-axis can be achieved using these excitation schemes. The movement towards the y-axis was not simulated, because of the symmetry of the actuator.

A frequency range from 27 to 63 kHz with a solution at 545 Hz intervals were chosen and adequate response curves of contact point's oscillation amplitudes and phases were calculated. The contact point is located at the middle of the top surface of the driving tip. The scheme used for excitation of the electrodes is illustrated in Fig. 1b. Results of calculations are given in Figs. 4a and b where the contact point's amplitude and phase

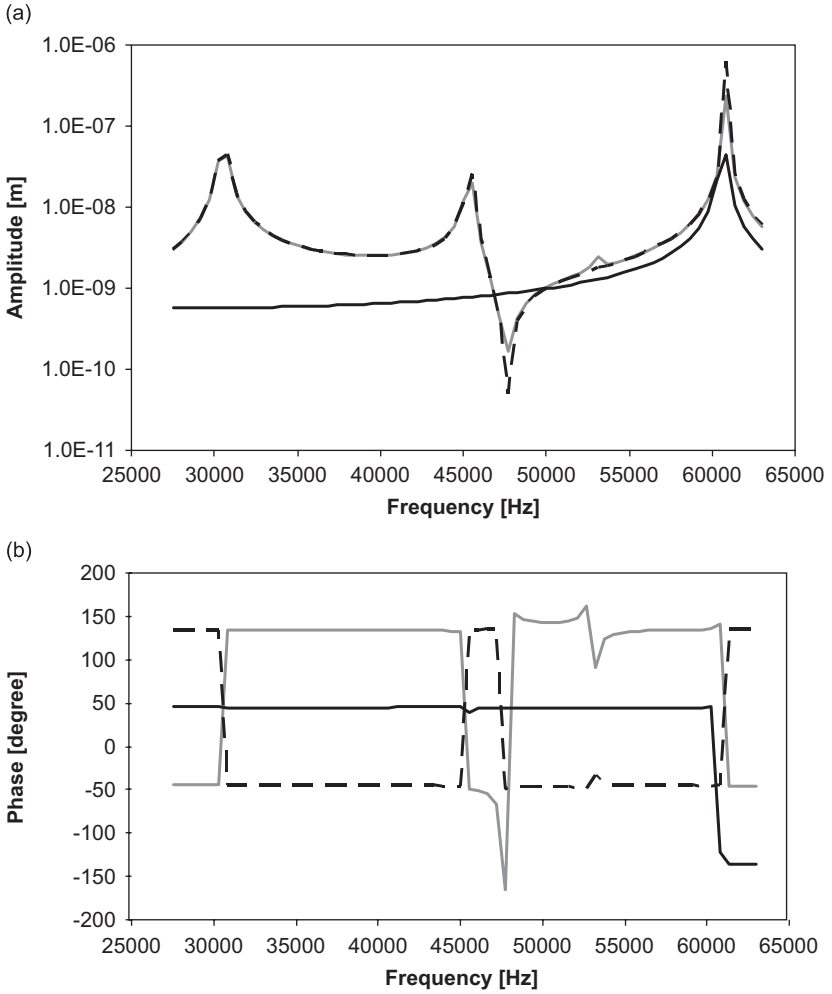

Fig. 4. Results of harmonic response analysis: (a) contact point's oscillation amplitude versus frequency; (b) contact point's oscillation phase versus frequency. ——, u_x; – –, u_y; ——, u_z.

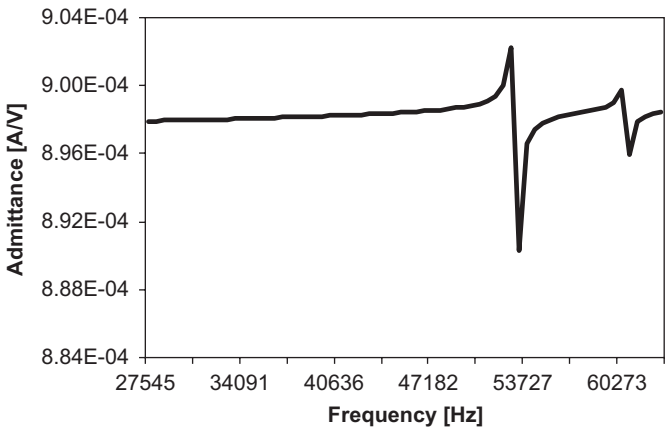

Fig. 5. Electrical input admittance versus frequency.

versus frequency are given. Graphs of contact point's oscillation amplitudes show that the excitation frequency at 30.8 and 60.8 kHz has local peaks and is very close to natural frequency Nos. 2 and 8, respectively. Also phase differences between graphs u_x, u_y and u_z significantly differ from 0 to π; therefore, these two frequencies were chosen as the input frequency of the piezoelectric actuator for calculations of contact point's trajectories.

Electrical input admittance over a frequency range of 27–63 kHz was calculated using Eq. (11). Results of the calculations are shown in Fig. 5. The admittance graph shows three resonant frequencies and two of them—30.8 and 60.8 kHz—coincide with resonant frequencies obtained from Figs. 4a and b. It confirms that excitation frequencies of the piezoelectric actuator for the calculations of the trajectories were selected rightly.

Calculations of the contact point's moving trajectories were done applying two excitation cases of the electrodes as shown in Figs. 1b and c. Totally six different input voltage frequencies, i.e. 30.2, 30.8, 31.3, 60.2,

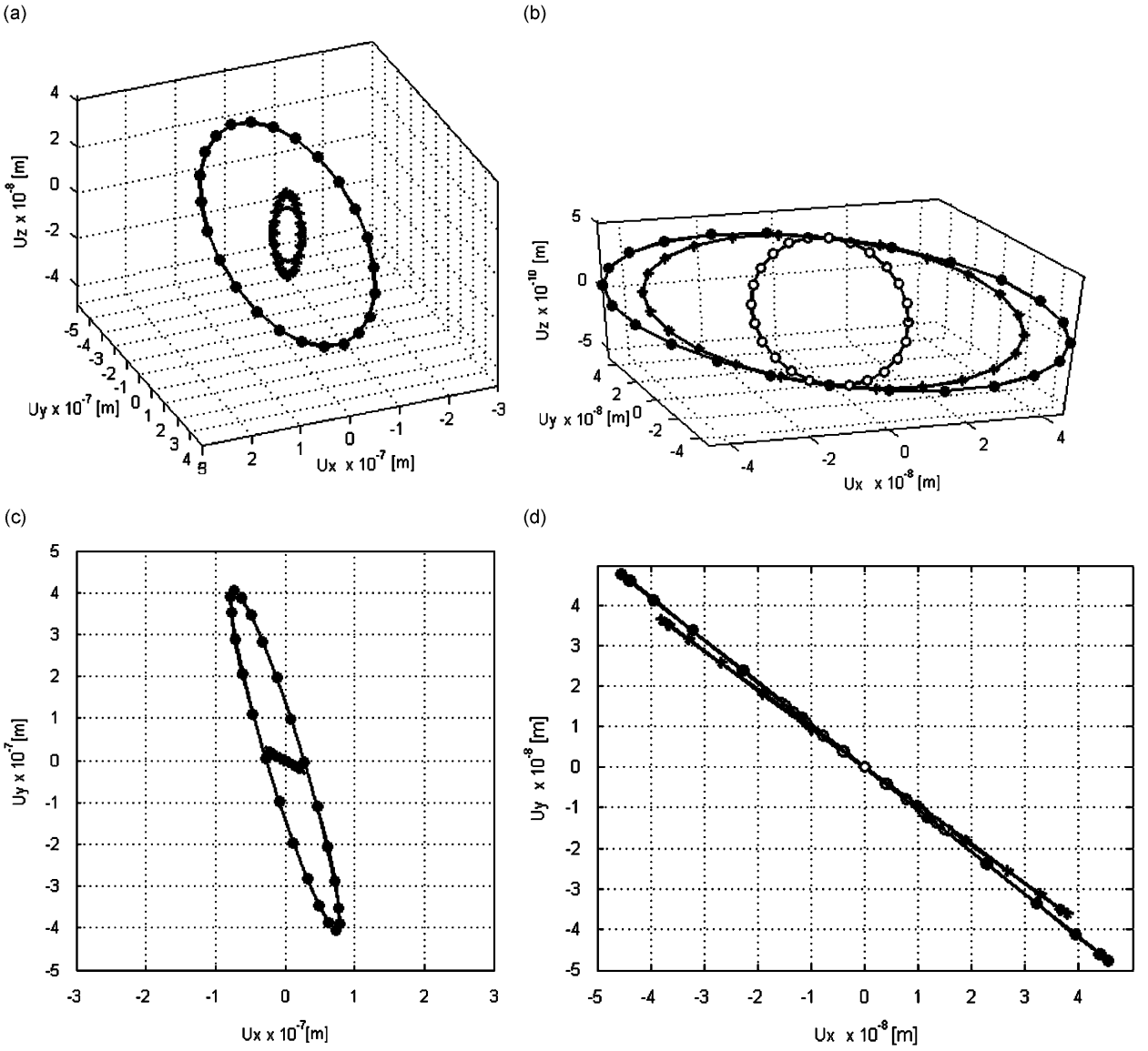

Fig. 6. Trajectories of contact point's movements for linear motion of slider in xy plane: (a) 3D view: —○—, 61.3 kHz; —●—, 60.8 kHz; —✳—, 60.2 kHz; (b) 3D view: —○—, 31.3 kHz; —●—, 30.8 kHz; —✳—, 30.2 kHz; (c) xy plane view: —○—, 61.3 kHz; —●—, 60.8 kHz; —✳—, 60.2 kHz; (d) xy plane view: —○—, 31.3 kHz; —●—, 30.8 kHz; —✳—, 30.2 kHz.

60.8 and 61.3 kHz were used to simulate the motion of the contact point. It allows us to compare parameters of trajectories and to define the best working frequency for the actuator. Figs. 6 and 7 illustrate trajectories of the contact point's movement under excitation schemes shown in Figs. 1b and c, respectively. It can be seen that trajectories have ellipsoidal shapes. Parameters of the ellipses are given in Table 2. All ellipses at 30 kHz range have a much larger ratio between the major and minor axes and smaller areas. It means that the contact point's motion and the strike, respectively, at 60 kHz is much more powerful than at 30 kHz and, therefore, the experimental study was performed analysing oscillations of the actuator at 60 kHz range.

From Figs. 6b and d it can be seen that major axes of ellipses are rotated about the centre of the coordinate system by the different angles and depend on excitation frequencies of the actuator. This can be explained because of difference in modal shapes that are actuated at these resonant frequencies.

Contact point's trajectories used for rotation of the slider are illustrated in Fig. 7. These trajectories are ellipsis, and energy of the contact point's motion at 60.8 kHz is much higher than at 30.8 kHz.

Numerical simulations have shown that the actuator has better contact point's motion characteristics at 60.8 kHz excitation frequency; therefore, simulations of the slider motion and experimental investigation will be done at this frequency. Numerical simulations of the piezoelectric actuator have shown that small changes of the electric input signal frequency significantly influence the contact point's movement characteristics.

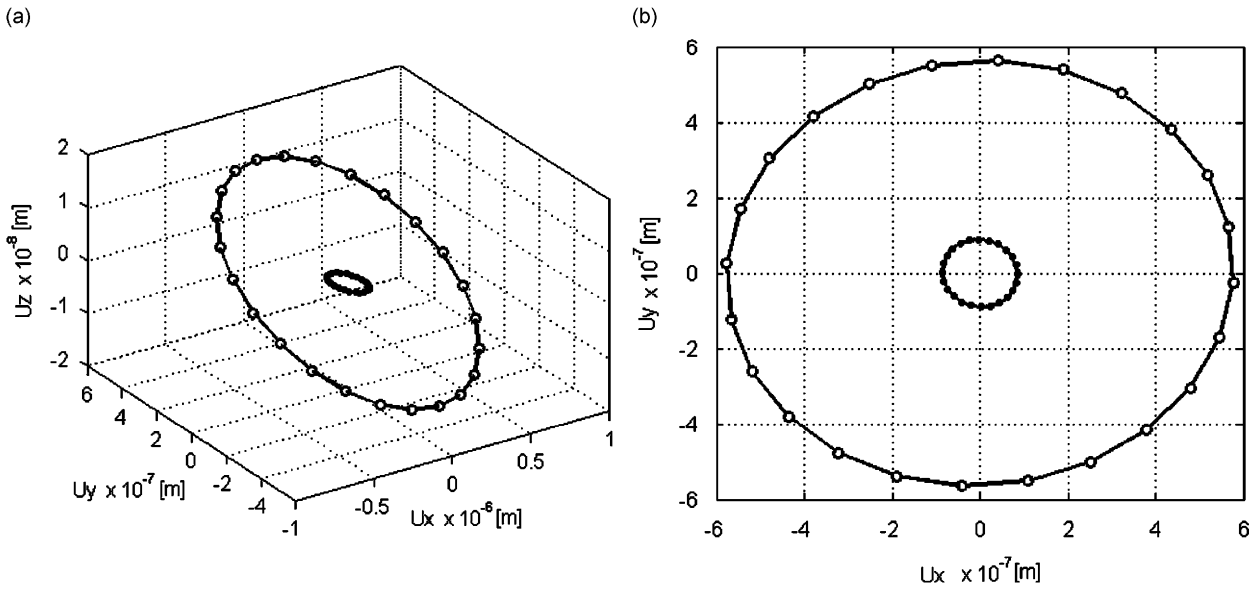

Fig. 7. Trajectories of contact point's movements when slider is rotating about z-axis: (a) 3D view; (b) xy plane view. —○—, 60.8 kHz; —●—, 30.8 kHz.

Table 2
Parameters of ellipses

Voltage frequency (kHz)	Major axis (μm)	Minor axis (μm)	Ratio	Area (m^2)
Excitation case (Fig. 1b)				
30.8	0.13182	0.001156	113.9	1.1977×10^{-16}
60.8	0.82085	0.11122	7.38	7.1707×10^{-14}
Excitation case (Fig. 1c)				
30.8	0.17035	0.17899	0.95	2.394×10^{-14}
60.8	1.12511	1.1603	0.96	1.0253×10^{-12}

4.2. Simulation of piezoelectric motor

A new finite element model of the piezoelectric motor was built, which is shown in Fig. 8. It consists of a piezoelectric actuator, a slider with a friction bar and a base block. This model involves nonlinear contact behaviour between the driving tip and the friction bar as well as the slider and the base block. Surface-to-surface contact elements TARGET170 and CONTA174 are employed to describe the contact problem in this simulation. Real constants in the contact pairs are defined in terms of the practical load case of the motor and are listed in Table 3 where contact pair No. 1 represents the contact between the driving tip and friction bar of the slider and contact pair No. 2 represents contact between the slider and base block. Two additional materials were used in this model. One is an aluminium alloy, which is employed to construct the slider and base block and another material is aluminium ceramic used for the friction bar of the slider.

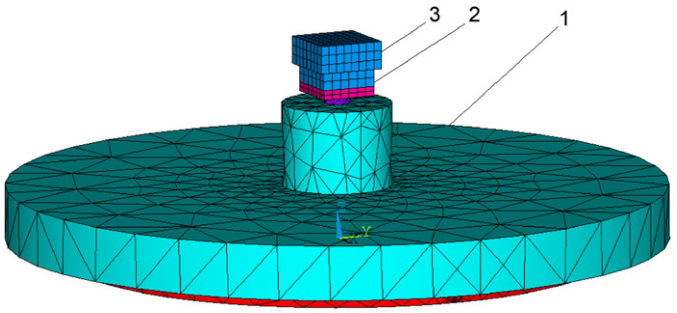

Fig. 8. Finite element model of piezoelectric motor: 1—actuator; 2—slider with friction bar; 3—base block.

Table 3
Parameters of contact pairs

Parameter	Pair No. 1	Pair No. 2
Contact stiffness, N/m	7.2×10^8	3.9×10^8
Penetration tolerance	0.1208	0.1896
Friction coefficient	0.35	0.02
Ratio of static/dynamic friction coefficient	2	10
Max friction stress, N/m^2	5000	500

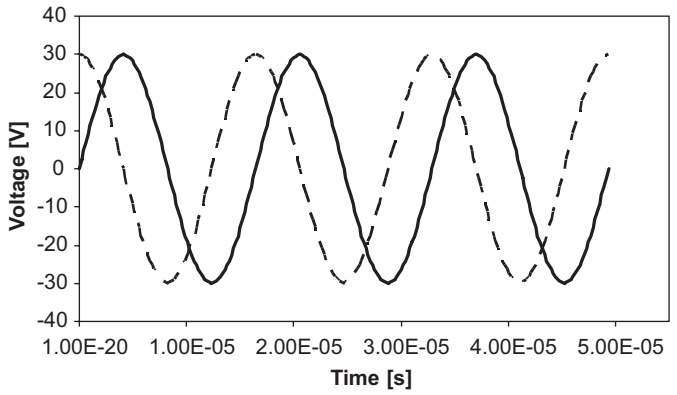

Fig. 9. Three cycles of loading case used in transient dynamic analysis: – –, voltage applied on first electrode; ——, voltage applied on opposite electrode.

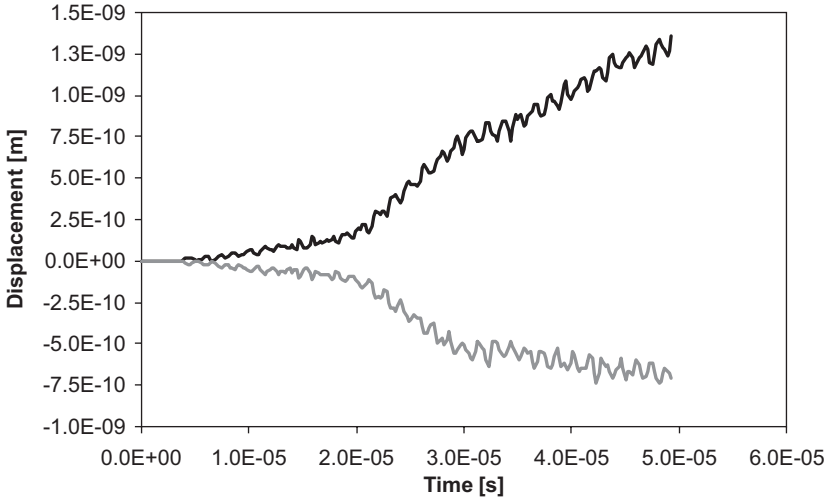

Fig. 10. Displacement curves of slider under three cycles load. ——, u_x; ——, u_y.

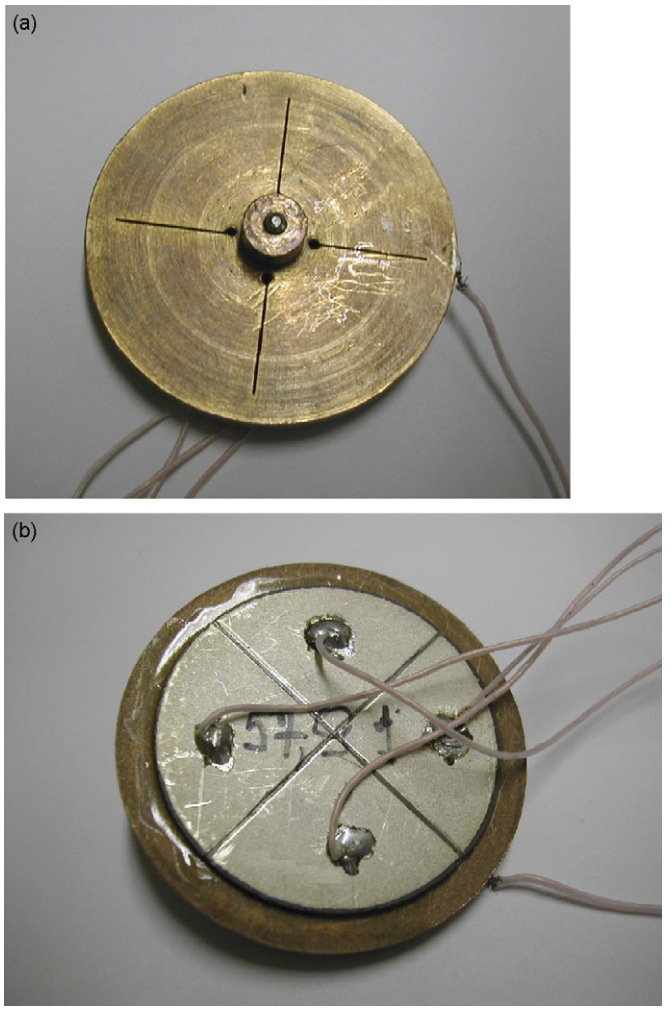

Fig. 11. Prototype actuator: (a) top view; (b) bottom view.

The finite element model of the piezoelectric motor is used in the transient dynamic analysis to investigate the transient process of the slider motion. The time-dependent loads are generated by sinusoidal voltage applied to two opposite electrodes. The frequency is specified at 60.8 kHz. In this simulation three cycles of time-dependent load are specified. Thus, the total time is 4.934×10^{-5} s. Curves of loads with three cycles are shown in Fig. 9. The integration time step is set at 2.0×10^{-7} s. Damping was ignored in the simulations. Results from these simulations are given in Fig. 10 where displacements of the slider in x- and y-direction under three cycles load are presented. From slider displacement curves that direction of the slider motion is rotated by 17.5°. The similar conclusion was done analysing elliptical trajectory of contact point motion from harmonic response analysis.

5. Experimental investigation

A prototype actuator, made for experimental studies, is shown in Fig. 11. The aims of this experiment were to verify results of numerical modelling, i.e. resonant frequencies and trajectories of the driven tip movement and to find a distribution of the oscillation amplitude on the top surface of the actuator. Amplitude–frequency characteristics of the actuator were determined with the help of the 4192A LF Impedance Analyzer (Hewlett Packard). Top surface's oscillations were measured using a vibrometer POLYTEC CLV 3D. The resonant frequency at 57.91 kHz was determined by means of electrical impedance study. The difference between experimental and numerical resonant frequencies is 4.75%.

Measurements of the actuator's top surface's oscillations were done using two excitation schemes of electrodes as shown in Figs. 1b and c. Results of measurements are given in Fig. 12; they confirm results of numerical modelling that the elliptical trajectory of the contact point can be achieved using this actuator. The distribution of oscillation amplitudes on the top surface of the actuator is the same as were obtained in numerical simulation. The difference between the contact point's oscillation amplitudes obtained in numerical modelling and measured in experiments is 5–8%.

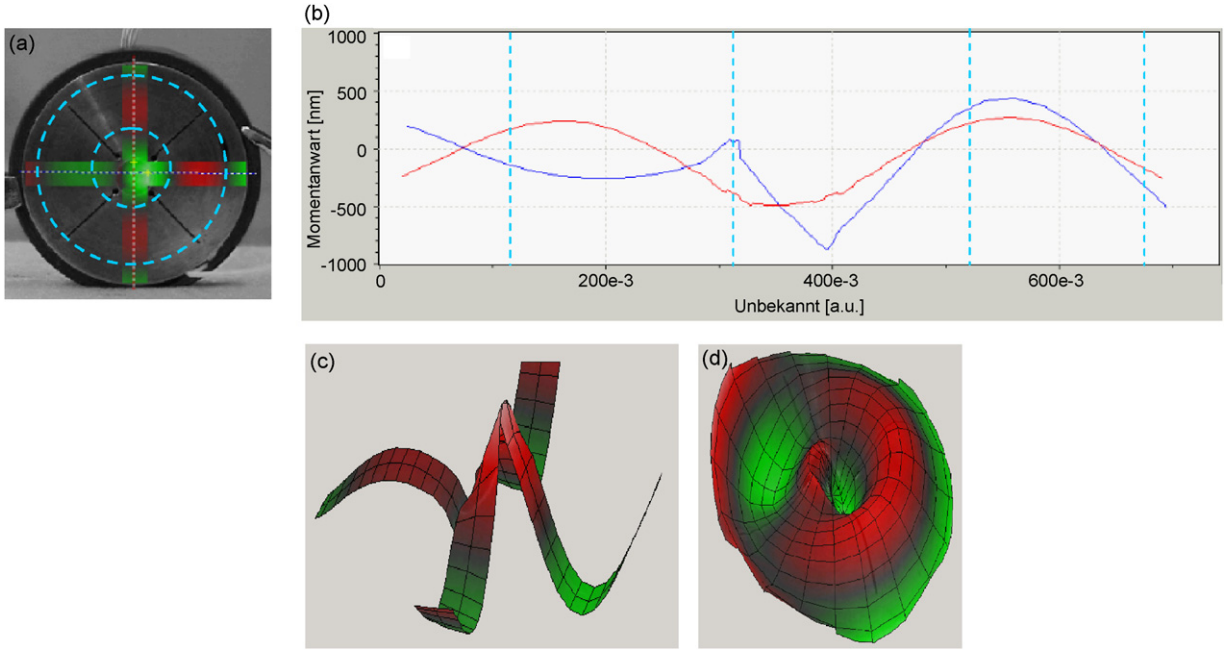

Fig. 12. Distribution of displacement amplitudes on the top surface of actuator at 57.91 kHz: (a) top surface view; (b) at the middle line of top surface; (c) 3D view; (d) at top surface of driven tip. Cases (a)–(c), used for linear motion, case (d) for rotation of slider.

6. Conclusions

A piezoelectric actuator of the novel design was developed for an omni-directional slider movement in the plane. Numerical and experimental studies confirm the possibility to achieve elliptical trajectories of driven tips and to move the slider using different excitation schemes of the piezoelectric actuator. Values of the resonant frequency and amplitudes from the finite element model are in good agreement with the experimental results.

References

[1] K. Uchino, *Piezoelectric Actuators and Ultrasonic Motors*, Kluwer Academic Publishers, Boston, Dordrech, London, 1997.
[2] T. Hemsel, J. Wallaschek, Survey of the present state of the art of piezoelectric linear motors, *Ultrasonics* 38 (2000) 37–40.
[3] S. Ueha, Y. Tomikawa, M. Kurosawa, K. Nakamura, *Ultrasonic Motors: Theory and Applications*, Clarendon Press, Oxford, 1993.
[4] R. Bansevicius, R. Barauskas, G. Kulvietis, K. Ragulskis, *Vibromotors for Precision Microrobots*, Hemisphere Publishing Corp., USA, 1988.
[5] M. Aoyagi, S.P. Beeby, N.M. White, A novel multi-degree-of-freedom thick-film ultrasonic motor, *IEEE Transactions on Ultrasonics, Ferroelectrics and Frequency Control* 49 (2) (2002) 151–158.
[6] Y. Gouda, K. Nakamura, S. Ueha, A miniaturization of the multi-degree-of-freedom ultrasonic actuator using a small cylinder fixed on a substrate, in: *Proceedings of the second International Workshop on Piezoelectric Materials and Applications in Actuators*, Paderborn, Germany, 2005, pp. 263–267.
[7] P. Vasiljev, S. Borodinas, S.-J. Yoon, D. Mazeika, G. Kulvietis, The actuator for micro moving of a body in a plane, *Materials Chemistry and Physics* 91 (1) (2005) 237–242.
[8] T. Morita, Miniature piezoelectric motors, *Sensors and Actuators* 103 (3) (2003) 291–300.
[9] P. Vasiljev, R. Bareikis, A. Rotmanas, D. Mazeika, G. Kulvietis, ultrasonic oscillatory System of "shaking beam" type, *Lithuanian Journal of Physics* 42 (5) (2002) 363–370.